Submission to Journal of Alloys and Compounds (June 2020)

Superior strength of tri-layered Al-Cu-Al nano-composites processed by high-pressure torsion

Piotr Bazarnik[a], Aleksandra Bartkowska[a], Barbara Romelczyk-Baishya[a], Bogusława Adamczyk-Cieślak[a], Jiaoyan Dai[b], Yi Huang[c,d], Małgorzata Lewandowska[a], Terence G. Langdon[d]

[a] Warsaw University of Technology, Faculty of Materials Science, Woloska 141, 02-507, PL
[b] School of Materials and Chemical Engineering, Ningbo University of Technology, Ningbo 315211, P.R. China
[c] Department of Design and Engineering, Faculty of Science and Technology, Bournemouth University, Poole, Dorset BH12 5BB, UK
[d] Materials Research Group, Faculty of Engineering and the Environment, University of Southampton, Southampton SO17 1BJ, UK

Abstract

This investigation demonstrates that a solid-state reaction occurs by the application of high-pressure torsion (HPT) in the production of nanostructured multilayered hybrid Al-Cu systems. Three-layered stacks of Al/Cu/Al were subjected for up to 200 revolutions of HPT under an applied pressure of 6.0 GPa. Microstructural and mechanical properties analysis were carried out after HPT using X-ray diffraction, scanning and transmission electron microscopy, energy dispersive spectrometry (EDX), microhardness measurements and tensile tests. The SEM observations revealed the formation of a multi-nano-layered structure in the whole volume of the disks. Further investigations with the use of TEM demonstrated that each nano-layer consists of nano-grains having sizes of about 20 nm. Analysis by XRD and selected area electron diffraction (SAED) confirmed the formation of intermetallic $CuAl_2$ and Cu_9Al_4 phases in the layered structures. The experiments also showed a significant improvement in microhardness (up to ~450 Hv) and tensile properties (over 900 MPa of UTS after 200 turns) when compared to both Al-1050 and 99.95%Cu alloys in the initial state and after HPT processing. The results demonstrate that HPT offers an outstanding opportunity for producing novel nanostructured Al-Cu multilayered composites having unique mechanical properties

Keywords: Al-Cu; high-pressure torsion; nano-composites; phase transformations; ultrafine grains.

*Corresponding author: Piotr Bazarnik (Piotr.Bazarnik @pw.edu.pl)

1. Introduction

The development of new and advanced materials is now driven by the technological demands of improved properties and wider functionalities as well as by numerous restrictions imposed by ecological considerations in various industrial applications [1]. Metals such as aluminium, copper and their alloys are now used extensively for many industrial applications and they will become principal future structural materials if their mechanical properties are sufficiently improved. In this respect, the fabrication of composites of aluminium and copper may meet the demands for higher strength and reductions in the overall weight. The Al-Cu hybrid materials appear attractive because of their low density and high thermal and electrical conductivity. They also exhibit higher strengths than other aluminium alloys.

Numerous methods are available for producing metal composites including diffusion bonding [2], powder metallurgy techniques [3] and explosive welding [4]. Nevertheless, it was shown recently that the use of severe plastic deformation (SPD) methods, including equal-channel angular pressing (ECAP) [5] and high-pressure torsion (HPT) [6], may be especially promising as fabrication techniques for the production of metal matrix nanocomposites [7-11]. These SPD techniques are attractive for the manufacturing of composite materials because they generally achieve very good bonding [12-14]. Of the various SPD methods now available, processing by HPT has the advantage of producing significant grain refinement [15,16], providing the capability of processing even hard-to-deform metals [17] or intermetallics [18] and, due to the high applied pressure and intense shear strain, producing phase transformations [19,20] or supersaturated solid solutions [21,22]. It is also well established that, by comparison with processing by ECAP, HPT produces smaller grains [23,24] and a higher fraction of grain boundaries having high angles of misorientation [25] and it has been used successfully for producing nanocomposites from metallic powders [14,26-29] and machining chips [30-33].

Recently an alternative approach was developed with HPT for the fabrication of high-performance hybrid materials by making use of the very high pressure to effectively join dissimilar bulk metals. The initial experiments were conducted using semi-circular disks of Ag-Ni [34], Nb-Zr [34], Al-Cu [35,36] and Mg-Al [37] or quarter disks of Al-Cu [38] and placing these pieces to form whole disks within the depression on the lower anvil of an HPT facility. Later, this approach was improved and further developed by stacking three whole disks of commercial Al and Mg alloys and then applying pressure and torsional straining to the stack [39]. This same approach was used in several later investigations using stacks of three or more disks of Al-Cu [40-44], Al-Fe [41,42,44], Al-Mg [21,41,42,45-50], Al-Mg-Cu-Fe-Ti [42], Al-Ti [41,42, 44], Cu-Al [51], Cu-Sn [52], Cu-Ta [22,53], Cu-ZnO [54], Fe-V [55,56], V-Zr [57] and Zn-Mg [58].

Recent investigations using stacks of Al and Cu disks demonstrated the potential for fabricating Al/Cu/Al composites by HPT after processing through up to a total of 60 turns [40,43,44]. These experiments confirmed the formation of a nanocrystalline structure and intermetallic phases of Al_2Cu, AlCu and Al_4Cu_9 but nevertheless the microstructures remained relatively inhomogeneous across the disk diameters even after 60 revolutions. Thus, the presence of the initial three-layered structure was essentially retained within the central region of the disk over a diameter of ~1.5 mm and this affected the microhardness values in the disk centre which, even after the HPT processing, remained close to the initial level for the commercial purity Cu.

The present investigation was motivated by these earlier results and by the opportunity to evaluate the potential for achieving greater homogeneity by conducting the HPT processing through larger numbers of revolutions. Accordingly, tests were conducted using HPT processing for up to a maximum of 200 turns and emphasis was placed on examining the quality

of bonding and the microstructural characterization in order to determine the origin of the exceptionally high strength of these hybrid materials.

2. Experimental material and procedures

The experiments were conducted using a commercial purity (CP) aluminium alloy (Al-1050, 99.95 wt.% Al) and CP copper (99.95%). The samples were received in the form of rods of 10 mm diameter and these Al and Cu rods were annealed for 1 h at 370°C and 480°C, respectively, in order to soften both materials. The rods were then cut into disks with thicknesses of 1.1 mm and ground to a final thickness of ~0.80 mm.

The HPT processing was conducted on stacks of three disks placed in the order of Al/Cu/Al and having a total thickness of ~2.4 mm. These disks were piled in the depression on the lower anvil of the HPT facility and then subjected to an applied pressure of 6.0 GPa at room temperature and torsional straining with a rotation speed of 1 rpm under quasi-constrained conditions where there is a small outflow of material around the periphery of the disk [59]. The disks were strained through total numbers of revolutions, N, of 20, 50, 150 and 200 turns. The anvils had a high roughness to prevent the sample from slipping during deformation. In addition, and for comparative purposes, separate disks of Al and Cu were tested through 10 revolutions of HPT under the same processing conditions.

The HPT-processed disks were initially examined by X-ray diffraction (XRD) using Bruker D8 Diskover and an energy for the emitter beam of 30 kV. The Co Kα X-Ray beam was filtered to form a point with a radius of 1 mm and all specimens were scanned on cross-sectional planes in the edge regions. Each sample was illuminated by high intensity hard X-rays for 5 s per step, the 2Θ angle was between 20° and 120° and the step size Δ2Θ was 0.025°.

Each HPT disk was then cut into two halves along a diameter using a diamond wafering saw and the cross-section of each disk was examined using optical microscopy (OM) and

scanning electron microscopy (SEM). Specimens for SEM observations were prepared using grinding and ion polishing with an Hitachi Ion Milling System IM-4000. The ion milling is a damage-free process and this polishing eliminates all deformation, stresses and oxide layers. Furthermore, the surface quality is sufficiently good to observe the structure using channelling contrast in an SEM microscope. Microstructural examination was carried out using an Hitachi SU-8000 SEM operated at 10 kV with a backscattered electron (BSE) detector. These microstructural observations were conducted in the central and periphery regions (approximately 1.0 mm from the edge) for each disk. Detailed microstructural observations of selected areas were performed using a CS-corrected dedicated scanning transmission electron microscope (STEM) Hitachi HD-2700 operating at an accelerating voltage of 200 kV. The STEM observations were carried out in the bright-field (BF) and high-angle annular dark field (HAADF) modes. Thin foils with a thickness of ~85 nm for STEM observations were extracted from the peripheral regions of each disk using a focused ion beam (FIB) system Hitachi NB 5000. Structural investigations were combined with advanced energy dispersive X-Ray (EDX) point and mapping analyses. The microstructures were also evaluated quantitatively using a computer-aided image analyser and the grain sizes were recorded in terms of the equivalent grain diameter, d_{eq}, defined as the diameter of a circle having a surface area equal to the surface area of the grain.

To evaluate the changes in mechanical properties due to HPT processing, microhardness tests were conducted on the cross-sections of disks using an FM-300 microhardness tester equipped with a Vickers indenter. Measurements were performed under a load of 100 g with a dwell time of 10 s and a spacing of 0.1 mm between each separate indentation. To determine the influence of HPT processing on the homogeneity of the structure, detailed microhardness measurements were performed on selected samples to permit the construction of color-coded microhardness maps.

These microhardness studies were complemented by tensile testing. Miniature tensile samples with gauge lengths of 2.5 mm were cut from off-centre positions in each disk using electro-discharge machining (EDM) [60]. The tensile tests were conducted at room temperature using a Zwick 005 universal testing machine under displacement control at an initial strain rate of 1.0×10^{-3} s^{-1}. For strain estimation, a Digital Image Correlation (DIC) was applied [61]. A charge-coupled device (CCD) camera operating at 4 fps with a Pentax lens was placed in front of the sample and the image acquisition with AVT software was synchronized with the beginning of each tensile test. The recorded images were analysed using VIC 2D software (Correlated Solutions) to create stress-strain maps. Based on the load-displacement data, the yield stress (YS), ultimate tensile stress (UTS) and elongation to failure were determined.

3. Experimental results

3.1. Microstructure and phase analysis after HPT

The OM images in Fig. 1 show the cross-sections of samples processed through 20, 50, 150 and 200 turns, respectively, where the bright regions denote the Al-rich phase and the dark regions correspond to the Cu-rich phase. Macroscopic observations confirmed that all samples were fully dense with no evidence for any macroscopic voids or delamination between the Al and Cu phases. In the disk after 20 turns the microstructure is of a gradient-type in the central section with clear evidence for the separate Al-rich and Cu-rich layers whereas in the outer regions of the disk the layered structure is fragmented due to the torsional straining and thin Cu layers or inclusions are evident within the Al phase. There is also a similar structural evolution after 50 turns but the overall size of the central layered structure is then reduced. A high degree of deformation is required to achieve a full intermixing of the Al and Cu layers throughout the

disk diameter and this is achieved after 150 and 200 revolutions where there is intermixing of the Al and Cu phases over the whole diameter and the microstructures are reasonably fully homogeneous.

Detailed structural investigations were carried out using SEM and Figs 2 and 3 show BSE images of the cross-sectional views at the disk centres and edges for the samples processed through 20 and 200 turns, respectively, where the brighter contrast corresponds to the Cu-rich regions and the darker contrast represents the Al-rich regions. The SEM images in Figs 2 and 3 generally confirm the observations by OM. For the sample after 20 turns, a layered Al/Cu/Al structure is present in the central region in Fig. 2(a) but with no evidence for voids or delamination. There is extensive grain refinement in Figs 2(b) and (c) with measured average grain sizes in the Al and Cu of ~650 and ~400 nm, respectively. By contrast, the average grain sizes in the separate Al and Cu disks were measured as ~700 and ~350 nm, respectively, after processing by HPT for 10 turns. In the outer parts of the disk in Figs 2(d) and (e), the SEM observations reveal significant fragmentation and a mixing of the Al and Cu layers. The higher magnification image in Fig. 2(e) also reveals evidence for shear bands and the formation of a lamellar structure with thin Cu-rich and Al-rich bands.

It appears that this lamellar structure evolves with increasing numbers of turns and for the sample after 200 turns in Fig. 3 there is a fine nano-layered structure throughout the whole diameter of the disk although in the central region in the upper and lower parts of the disk it is apparent that the material is not fully mixed as marked in Fig. 3(a). In the outer regions of the disk there is a full mixing of Al and Cu over the entire thickness as in Fig. 3(c). Although there remains evidence for the lamellar structure in Fig. 3(d), the thicknesses of the individual Al-rich and Cu-rich bands are smaller than after 20 revolutions. In addition, some contrast changes are visible in the BSE image in Fig. 3(e) which suggests the possible formation of new phases.

A detailed structural investigation was conducted from the edge regions using STEM techniques and Figs 4 and 5 show STEM images for the samples processed through 20 and 200 revolutions, respectively. After 20 turns the structure consists of ultra-thin Al-rich and Cu-rich layers as in Fig. 4(a) with evidence for extensive grain refinement in all layers. Measurements showed the grains in the Al layers are elongated and smaller (~230 ± 20 nm) than in the Cu bands where the grain size is strongly affected by the thickness of individual layers and reaches sizes of up to ~310 ± 70 nm. High magnification observations confirmed, as in Figs 4(b) and (c), that the interface-affected zone on the contact surface of the Al and Cu layers is formed during HPT processing. Furthermore, there is a diffusion zone on the contact surface of nanolayers in Fig. 4(c) which was also confirmed by line EDX analysis as in Fig. 4(d). This diffusion effect was observed on almost all Al-Cu interfaces. In addition, in some places, the thinnest copper layers have transformed into nanometer-sized grains as in Fig. 4(b) with sizes of ~30 ± 20 nm.

There is a further decrease in grain size after 200 turns as in Fig. 5(a) but the lamellar structure remains as in Fig. 5(b). Measurements revealed a bimodal character of the microstructure with Al-rich grains of ~95 ± 15 nm in Fig. 5(c) and Cu-rich grains in the range of ~5 - 20 nm. Chemical composition analysis, as in Fig. 5(d), revealed a high concentration of Cu in these nano-sized bands although Cu was also present in the Al matrix in the form of a solid supersaturated solution. Rings in the selected area electron diffraction (SAED) patterns as in Fig. 6(a) confirmed the presence of Al and Cu as well as the formation of the Al_2Cu and Al_4Cu_9 phases where dark field imaging from the Al_2Cu (110) ring as in Fig. 6(b) confirmed that this phase occurs primarily in the Cu-rich nano-sized bands. The presence of these intermetallic phases is consistent with earlier reports [40,43]. A quantitative image correlation analysis of several dark field images after 200 turns showed that the fraction of the intermetallic

Al_2Cu phase is about 9.7%. The diffraction rings from the Al_4Cu_9 phase were too weak to conduct any quantitative analysis.

The phase compositions were also examined by XRD analysis and the patterns for the initial materials and after processing from 20 to 200 turns are shown in Fig. 7. These patterns reveal a significant broadening of the peaks due to the severe grain refinement, with the broadening becoming more intense after increasing numbers of turns. The patterns confirm the presence of the Al and Cu phases and the formation of the Al_2Cu and Al_4Cu_9 phases. These latter phases are visible even after 20 turns but the peaks become more intensive with increasing numbers of turns. A semiquantitative analysis of the XRD patterns gave estimates for the fractions of the intermetallic Al_2Cu and Al_4Cu_9 phases at 2.5%, 4.4%, 6.9% and 10.2% after 20, 50, 150 and 200 turns, respectively. It should be noted that phase calculations from XRD can be affected by many factors such as severe grain refinement, internal stresses and texture. Nevertheless, the result for the sample after 200 turns is reasonably consistent with the earlier estimate using the dark field images.

3.2. Mechanical properties

The distributions of the Vickers microhardness on one-half of the cross-sections of the disks is shown in the color-coded contour maps in Fig. 8 after processing by HPT through 20, 50, 150 and 200 turns: the values of the microhardness are given in the colour key on the right and the distributions are plotted with the centre of the disk lying along the left axis. For comparison, the reference samples of Cu and Al showed average Vickers microhardness values of ~80 and ~25 Hv, respectively, for the as-annealed states and ~130 and ~50 Hv, respectively, after HPT for 10 turns.

Inspection of Fig. 8 shows that the microhardness of the multilayered composite increases significantly with increasing numbers of turns. The hardness values in the edge region are ~260 Hv after only 20 turns but in the central region the hardness values are in the range of ~50–130 Hv which is close to the initial values. This is consistent with earlier work on the Al/Cu/Al system where there was little or no significant increase in hardness in the central region after processing up to 60 turns [40,43]. In addition, the highest hardness values of ~110–130 Hv were recorded primarily in the Cu layers whereas the hardness was lower at ~50 Hv in the Al layers. The radius of the central zone of inhomogeneity extended through approximately 3 mm after 20 turns but this was reduced to ~2 mm after 50 turns and the hardness near the edge then increased to ~350 Hv. Further processing up to 150 turns gave an additional hardness increase up to ~400 Hv but with some small areas of lower hardness near the centre of the disk. Finally, after 200 turns the microhardness was fairly homogeneous throughout the disk with an average value of ~350 Hv but with highest hardness values of ~450 Hv near the outer edge of the disk. This hardness is exceptionally high by comparison with the initial hardness values of the pure Cu and pure Al in the as-annealed state and after HPT processing for 10 turns.

The results of tensile testing for the HPT-processed hybrid materials are illustrated in Fig. 9 where these data are complemented by including results for Cu and Al samples both in an as-annealed state and after 10 HPT revolutions. For convenience, the results are also summarized in Table 1 showing the yield strength (YS), the ultimate tensile strength (UTS) and the elongation to failure. These tensile tests demonstrate that the Al-Cu-Al composites exhibit very high strength with values for the UTS after 20 and 50 turns of ~420 ± 20 and ~460 ± 24 MPa, respectively. These results are much higher than the conventional values anticipated for Cu and Al in an as-annealed state and for Al after HPT processing but they are close to the values for Cu after HPT for 10 turns (525 ± 10 MPa). With additional HPT turns, the strength increases further and reaches extremely high strength values of ~710 and ~910 MPa for the samples

processed through 150 and 200 revolutions, respectively. Nevertheless, these hybrid materials exhibit high strength but only limited elongations to failure of about 2%.

4. Discussion

The results from this investigation demonstrate the potential for fabricating aluminium-based hybrid material by using conventional quasi-constrained HPT processing with a stack of disks consisting of commercial purity Al and Cu. By HPT processing through 200 turns, which is far in excess of the 60 turns used in earlier investigations [40,43,44], it was possible to form a unique multi-layered structure which was reasonably homogeneous throughout the entire disk, both in the radial direction and on cross-sectional planes, without any visible porosity or the presence of any delamination between the layers. The results demonstrate instead the development of a fine dispersion of Cu-rich phases within a nanostructured Al matrix and with rapid diffusion of Cu to Al and the consequent formation of intermetallic phases such as Al_2Cu and Al_4Cu_9.

Careful examination of samples suggests that the mixing effect, especially in the central part of the disks, may have been enhanced by a slight misalignment between the upper and lower anvils, as marked on Fig. 3(a), where two unmixed areas in the disk correspond to the centres of the upper and lower anvils. This proposal is reasonable because it is well established that anvil misalignments of the order of 100 or 200 μm may have significant effects on the flow properties within the HPT-processed samples [62-64]. As a result, a fully mixed structure with a thin lamellar configuration was observed in the central region after 150 revolutions and further processing up to 200 turns led to an additional reduction in the lamellar thickness. At the same time, there was a significant reduction in grain size below ~100 nm within the Al matrix after processing. This is a unique result especially when compared with data reported for conventional Al-Cu alloys after SPD processing [65-72]. A progressive mixing of phases with an accompanying reduction in lamellar thickness, accompanied also by significant grain size

reductions, was observed also for other hybrid systems processed by HPT such as Al-Mg [45], steel-V [55], Cu-Ta [22,53], Al-Fe [44], Mg-Zn [58] and Al-Ti [44].

The initial objective of using HPT in these systems was to facilitate the formation of nano-sized intermetallic phases which will improve and strengthen the mechanical properties of the composites. An additional advantage of HPT or other SPD techniques is that the materials exhibit significantly higher diffusion coefficients due to the introduction by processing of high populations of lattice defects [35,73-75]. This effect is especially visible in the Al-Cu interfacial zones as in Fig. 4 where there was evidence for diffusion of Cu and Al elements on the surface contact of nanolayers. As a consequence, the intermetallic Al_2Cu and Al_4Cu_9 phases are formed at the interfacial zones where these phase transformations are favoured in the joining zones of the Al-rich and Cu-rich regions [35,40,51,76]. Further deformation leads to a significant increase in the fraction of intermetallic phases which are located mainly in the Cu-rich regions.

It is important to examine the kinetics of formation of these intermetallic phases. For the Al-Cu system, saturated solid solutions Al(Cu) and Cu(Al) firstly form on each side due to mutual diffusion. Since the solubility limit of Cu in Al is almost two orders of magnitude smaller than that of Al in Cu [77,78], the Al(Cu) solid solution is expected to saturate first. Moreover, the diffusion coefficient of Cu in Al is much higher than for Al in Cu ($D_{Cu} \approx 1.78 \times 10^{-15}\ m^2 \cdot s^{-1}$ and $D_{Al} \approx 6.54 \times 10^{-19}\ m^2 \cdot s^{-1}$) [78]. Thus, the Cu atoms can diffuse to the Al side rapidly so that the Al side becomes oversaturated and subsequently Al_2Cu will form at the interfacial zone. At the same time, the Al_2Cu phase has the most negative effect of Gibbs free energy (−15.8 (J/mol)) of formation and from the thermodynamic point of view it will be the first phase formed at the Al-Cu interfacial zone [79]. By contrast the negative energy for the Al_4Cu_9 phase is -19.7 (J/mol) [79] which makes it a less-favoured phase for formation. This explains the reason for the Al_2Cu phase occurring mainly in this hybrid system (Fig. 6 and 7). It should be mentioned that the diffusion is controlled primarily by the temperature of the

processing, and since in this study the HPT process was conducted at room temperature the fast diffusion on the contact surfaces was induced only by the shear deformation at the Al-Cu interfacial zones in order to maintain unity of the system. This was a direct consequence of the differences in strength and Young's modulus for the individual layers.

As shown in Figs 8 and 9, extreme increases in hardness and strength were observed in the hybrid materials synthesized in this study. The hardness of the HPT-processed Al-Cu system approached ~450 Hv after 200 HPT turns and this is significantly higher than the hardness of nanocrystalline aluminium (~50 Hv) and copper (~130 Hv). Furthermore, a high structural homogenisation was observed across the disk diameter after 200 revolutions and this had a major impact on the values of the Vickers microhardness which were reasonably similar across the disk diameter. The UTS of the hybrid material exceeded 900 MPa which is an order of magnitude higher than for the unprocessed aluminium (~90 MPa) and more than three times higher than for the unprocessed copper (~280 MPa). Such intense hardening was also reported earlier for other hybrid systems synthesized by HPT such as the Cu-Ta system [22,53] where the hardness after HPT was four times higher than for the initial material or the Al-Mg system [42-47] where the hardness after HPT was three times higher.

Based on these results, it is reasonable to assume that in hybrid systems produced by HPT processing the overall strength of the material is not governed exclusively by the grain refinement through the Hall-Petch relationship [80,81] but there is, in addition, a combination of various other strengthening mechanisms such as solid solution strengthening and precipitation hardening [82]. The value of the hardness increase based on the Hall-Petch relationship and solid solution strengthening may be expressed by the following equation [39]:

$$\Delta Hv = 1/3[H(wt.\%\, Cu) + Ho + kd^{-0.5}] \quad (1)$$

where H_o, H and k are material constants and d is the average grain size and, using the general relationship between yield strength (MPa) and hardness (Hv), Hv = $\sigma_y/3$ [83]. The solution strengthening from Cu in the Al matrix has a negligible effect in this case since it is only 7 MPa for each weight percent of Cu [84]. The strength from the presence of precipitates can be estimated from the Orowan model [85] which plays a significant role in the strengthening of composite materials [85,86]. Thus, the hardening effect from precipitates may be expressed by the following equation:

$$\Delta Hv_{prec} = \frac{Gb}{\pi}\left\{\frac{1}{d(1-\sqrt{f})}\left[\frac{d\sqrt{f}}{d_{prec}} ln\frac{d_{prec}}{r_0} + \ln d\right] - \frac{1}{d} ln\frac{d}{r_0}\right\} \quad (2)$$

where G and b are the shear modulus (27 GPa) and the Burgers vector (0.274 nm) of the matrix element, respectively, r is the core cut-off radius in the dislocation line energy which is taken as ~1 nm, d_{prec} is the size of the reinforcing Al_2Cu and Al_4Cu_9 phases and f is the fraction of these strengthening phases. In practice dislocation strengthening should also be considered as an active mechanism. However, because the structure of these materials was very complex and contained many nano elements, the dislocation density was only roughly determined and the sample after 200 revolutions revealed a large scatter of σ_{ds} = 50–100 MPa. Using data obtained in this study in equations (1) and (2) permits a direct estimate of the microhardness of the fabricated hybrid composites.

Using this approach and taking ~0.9% of Cu in the matrix as solid solution, $d \approx 240$ nm, $d_{prec} \approx 30$ nm and f ≈ 2.5%, the microhardness of the disk after 20 turns is calculated as Hv ≈ 224 ± 30. After 200 turns and taking ~5.65% of Cu in the matrix as solid solution, $d \approx 90$ nm, $d_{prec} \approx 15$ nm and f = 10.2%, the microhardness is calculated as Hv ≈ 435 ± 35. Both results are in excellent agreement with the experimental results as documented in Fig. 8. In practice, the presence of the intermetallic phases makes the largest contribution to the overall microhardness and for the sample processed through 200 turns this contribution is more than 50%.

The results presented in this study on the mechanical bonding of dissimilar metals by HPT demonstrates a very significant potential for the synthesis of nanocrystalline intermetallic-strengthened hybrid materials exhibiting extraordinary mechanical properties. It appears that the deformation-induced bonding of the Al and Cu phases gives a multi-layered structure and thereby provides a major driving force for the formation of the Al_2Cu and Al_4Cu_9 intermetallic phases. It is reasonable to anticipate the occurrence of similar effects when processing other dissimilar metal disks.

5. Summary and conclusions

- The synthesis of a new Al–Cu alloy system was demonstrated using conventional HPT processing at room temperature under 6.0 GPa at 1 rpm.
- HPT of the initial stack of Al-Cu-Al resulted in a strong joining of all layers, a fragmentation of Al and Cu layers, and their mixing and formation of a fine lamellar structure.
- HPT processing of this bimetallic system led to a strong grain refinement down to a grain size of ~10-20 nm which was accompanied by a very high microhardness and tensile results of about ~450 Hv and ~910 MPa of UTS.
- HPT promotes the solid-state reaction of Al and Cu elements so that there is the formation of Al_2Cu and Al_4Cu_9 phases as well as the dissolution of Al and Cu components in each matrix
- The major contribution to the overall strength or hardness is given by the intermetallic nanoparticles and it was estimated at about 50%.

Acknowledgments

This work was carried out within a SONATINA 1 project: “Synthesis of novel hybrid materials using High-Pressure Torsion” financed by the Polish National Science Centre (Contract No. UMO-2017/24/C/ST8/00145). The work of three authors was supported by the European Research Council under ERC Grant Agreement No. 267464-SPDMETALS (JD, YH and TGL).

References

[1] K. Lu, The future of metals, Science, 328 (2010) 319-320.

[2] J. Cao, J. Liu, X. Song, X. Lin, J. Feng, Diffusion bonding of TiAl inter-metallic and Ti_3AlC_2 ceramic: interfacial Microstructure and joining properties, Mater. Des., 56 (2014) 115-121.

[3] J.W. Kaczmar, K. Pietrzak, W. Włosiński, The production and application of metal matrix composite materials, J. Mater. Process. Technol., 106 (2000) 58-67.

[4] P. Bazarnik, B. Adamczyk-Cieślak, A. Gałka, B. Płonka, L. Śnieżek, M. Cantoni, M. Lewandowska, Mechanical and microstructural characteristics of Ti6Al4V/AA2519 and Ti6Al4V/AA1050/AA2519 laminates manufactured by explosive welding, Mater. Des., 111 (2016) 146-157.

[5] R.Z. Valiev, T.G. Langdon, Principles of equal-channel angular pressing as a processing tool for grain refinement, Prog. Mater. Sci., 51 (2006) 881-981.

[6] A.P. Zhilyaev, T.G. Langdon, Using high-pressure torsion for metal processing: Fundamentals and applications, Prog. Mater. Sci., 53 (2008) 893-979.

[7] Y. Huang, P. Bazarnik, D. Wan, D. Luo, P.H.R. Pereira, M. Lewandowska, J. Yao, B. E. Hayden, T.G. Langdon, The fabrication of graphene-reinforced Al-based nanocomposites using high-pressure torsion, Acta Mater., 164 (2019) 499-511, https://doi.org/10.1016/j.actamat.2018.10.060

[8] S.N. Alhajeri, K.J. Al-Fadhalah, A.I. Almazrouee, T.G. Langdon, Microstructure and microhardness of an Al-6061 metal matrix composite processed by high-pressure torsion, Mater. Charact., 118 (2016) 270-278, https://doi.org/10.1016/j.matchar.2016.06.003

[9] M. Kawasaki, Y. Huang, C. Xu, M. Furukawa, Z. Horita, T.G. Langdon, A quantitative study of cavity development in the tensile testing of an aluminum metal matrix composite processed by equal-channel angular pressing, Mater. Sci. Eng. A, 410–411 (2005) 402-407

[10] Y.Z. Tian, S.D. Wu, Z.F. Zhang, R.B. Figueiredo, N. Gao, T.G. Langdon, Microstructural evolution and mechanical properties of a two-phase Cu–Ag alloy processed by high-pressure torsion to ultrahigh strains, Acta Mater., 59 (2011) 2783-2796

[11] M. R. Akbarpour, H. Mousa Mirabad, S. Alipour, H. S. Kim, Enhanced tensile properties and electrical conductivity of Cu-CNT nanocomposites processed via the combination of flake powder metallurgy and high pressure torsion methods, Mater. Sci. Eng. A, 773 (2020) 138888

[12] L. Bian, W. Liang, G. Xie, W. Zhang, J. Xue, Enhanced ductility in an Al–Mg2Si in situ composite processed by ECAP using a modified BC route, Mater. Sci. Eng. A, 528 (2011) 3463-3467

[13] I. Sabirov, R. Pippan, Formation of a W–25% Cu nanocomposite during high pressure torsion, Scr. Mater., 52 (2005) 1293-1298

[14] P. Bazarnik, S. Nosewicz, B. Romelczyk-Baishya, M. Chmielewski, A. Strojny Nędza, J. Maj, Y. Huang, M. Lewandowska, T. G. Langdon, Effect of spark plasma sintering and high-pressure torsion on the microstructural and mechanical properties of a Cu–SiC composite, Mater. Sci. Eng. A, 766 (2019) 138350

[15] P. Bazarnik, Y. Huang, M. Lewandowska, T.G. Langdon, Structural impact on the Hall–Petch relationship in an Al–5Mg alloy processed by high-pressure torsion, Mater. Sci. Eng. A, 626 (2015) 9-15

[16] P. Bazarnik, Y. Huang, M. Lewandowska, T.G. Langdon, Enhanced grain refinement and microhardness by hybrid processing using hydrostatic extrusion and high-pressure torsion, Mater. Sci. Eng. A, 712 (2018) 513-520

[17] Y. Huang, R.B. Figueiredo, T. Baudin, F. Brisset, T.G. Langdon, Evolution of Strength and Homogeneity in a Magnesium AZ31 Alloy Processed by High-Pressure Torsion at Different Temperatures, Adv. Eng. Mater. 14 (2012) 1018-1026

[18] K. Edalati, S. Toh, M Watanabe, Z Horita, In situ production of bulk intermetallic-based nanocomposites and nanostructured intermetallics by high-pressure torsion, Scripta Mater., 66 (2012) 386-389

[19] Y. Sun, M. Aindow, R. J. Hebert, T. G. Langdon, E. J. Lavernia, High-pressure torsion-induced phase transformations and grain refinement in Al/Ti composites, J. Mater. Sci., 52 (2017) 12170-12184.

[20] A. Bachmaier, R. Pippan, High-Pressure Torsion Deformation Induced Phase Transformations and Formations: New Material Combinations and Advanced Properties, Mater. Trans., 60 (2019) 1256-1269

[21] J.-. Han, K.-D. Liss, T.G. Langdon, M. Kawasaki, Synthesis of a bulk nanostructured metastable Al alloy with extreme supersaturation of Mg, Sci. Reports 9 (2019) 17186

[22] T. Mousavi, J. Dai, P. Bazarnik, P.H.R. Pereira, Y. Huang, M. Lewandowska, T.G. Langdon, Fabrication and characterization of nanostructured immiscible Cu–Ta alloys processed by high-pressure torsion, J. Alloys Comp.832 (2020) 155007

[23] A.P. Zhilyaev, B.-K.Kim, G.V. Nurislamova, M.D.Baró, J.A.Szpunar, T.G.Langdon, Orientation imaging microscopy of ultrafine-grained nickel, Scripta Mater. 46 (2002) 575-580

[24] A.P. Zhilyaev, G.V. Nurislamova, B.-K. Kim, M.D. Baró, J.A. Szpunar, T.G. Langdon, Experimental parameters influencing grain refinement and microstructural evolution during high-pressure torsion, Acta Mater. 51 (2003) 753-765

[25] J. Wongsa-Ngam, M. Kawasaki, T.G. Langdon, A comparison of microstructures and mechanical properties in a Cu–Zr alloy processed using different SPD techniques, J. Mater. Sci., 48 (2013) 4653-4660

[26] V. V Stolyarov, Y. T Zhu, T. C Lowe, R. K Islamgaliev, R. Z Valiev, Processing nanocrystalline Ti and its nanocomposites from micrometer-sized Ti powder using high pressure torsion, Mater. Sci. Eng. A,282 (2000) 78-85, https://doi.org/10.1016/S0921-5093(99)00764-9

[27] R. Kulagin, A. Mazilkin, Y. Beygelzimer, D. Savvakin, I. Zverkova, D. Oryshych, H. Hahn, Influence of High Pressure Torsion on structure and properties of Zr-Ti-Nb alloy synthesized from TiH2, ZrH2 and Nb powders, Mater. Lett. 233 (2018) 31-34

[28] A.P. Zhilyaev, G. Ringot, Y. Huang, J.M. Cabrera, T.G. Langdon, Mechanical behavior and microstructure properties of titanium powder consolidated by high-pressure torsion, Mater. Sci. Eng. A, 688 (2017) 498-504, https://doi.org/10.1016/j.msea.2017.02.032

[29] C. Silva, L.A. Montoro, D.A.A. Martins, P.A. Machado, P.H.R. Pereira, B.M. Gonzalez, T.G. Langdon, R.B. Figueiredo, A. Isaac, Interface structures in Al-Nb2O5 nanocomposites processed by high-pressure torsion at room temperature, Mater. Charact., 162 (2020) 110222

[30] A. P. Zhilyaev, A. A. Gimazov, G. I. Raab, T. G. Langdon, Using high-pressure torsion for the cold-consolidation of copper chips produced by machining, Mater. Sci. Eng. A, 486 (2008) 123-126

[31] M.M. Castro, A.P. Carvalho, P.H.R. Pereira, A.C.I. Neta, R.B. Figueiredo, T.G. Langdon, Consolidation of Magnesium and Magnesium Alloy Machine Chips Using High-Pressure Torsion, Mater. Sci. Forum, 941 (2018) 851-856

[32] M.M. Castro, P.H.R. Pereira, A. Isaac, R.B. Figueiredo, T.G. Langdon, Development of a magnesium-alumina composite through cold consolidation of machining chips by high-pressure torsion, J. Alloys Compd., 780 (2019) 422-427

[33] M.M. Castro, P.H.R. Pereira, R.B. Figueiredo, T.G. Langdon, Developing magnesium-based composites through high-pressure torsion, Letters Mater. 9 (2019) 541-545

[34] T. Miyazaki, D. Terada, Y. Miyajima, C. Suryanarayana, R. Murao, Y. Yokoyama, K. Sugiyama, M. Umemoto, Y. Todaka, N. Tsuji, Synthesis of non-equilibrium phases in immiscible metals mechanically mixed by high pressure torsion, J. Mater. Sci. 46 (2011) 4296–4301.

[35] K. Oh-ishi, K. Edalati, H.S. Kim, K. Hono, Z. Horita, High-pressure torsion for enhanced atomic diffusion and promoting solid-state reactions in the aluminum–copper system, Acta Mater. 61 (2013) 3482–3489.

[36] R. Kulagin, Y. Beygelzimer, Yu. Ivanisenko, A. Mazilkin, B. Straumal, H. Hahn, Instabilities of interfaces between dissimilar metals induced by high pressure torsion, Mater. Lett., 222 (2018) 172-175

[37] M.M. Castro, S. Sabbaghianrad, P.H.R. Pereira, E.M. Mazzer, A. Isaac, T.G. Langdon, R.B. Figueiredo, A magnesium-aluminium composite produced by high-pressure torsion, J. Alloys Compd. 804 (2019) 421-426.

[38] O. Bouaziz, H. S. Kim, Y. Estrin, Architecturing of Metal-Based Composites with Concurrent Nanostructuring: A New Paradigm of Materials Design. Adv. Eng. Mater., 15 (2013) 336-340

[39] B. Ahn, A.P. Zhilyaev, H.-J. Lee, M. Kawasaki, T.G. Langdon, Rapid synthesis of an extra hard metal matrix nanocomposite at ambient temperature, Mater. Sci. Eng. A, 635 (2015) 109-117

[40] J.-K. Han, D.K. Han, G. Y. Liang, J.-I. Jang, T.G. Langdon, M. Kawasaki, Direct Bonding of Aluminum–Copper Metals through High-Pressure Torsion Processing, Adv. Eng. Mater., 20 (2018) 1800642

[41] J.-K. Han, J.-il Jang, T.G. Langdon, M. Kawasaki, Bulk-State Reactions and Improving the Mechanical Properties of Metals through High-Pressure Torsion, Mater. Trans. 60 (2019) 1131-1138

[42] J.-K. Han, T. Herndon, J.-I. Jang, T.G. Langdon, M. Kawasaki, Synthesis of Hybrid Nanocrystalline Alloys by Mechanical Bonding through High-Pressure Torsion, Adv. Eng. Mater., 22 (2020) 1901289

[43] G.F. Korznikova, R. Kabirov, K. Nazarov, R. Khisamov, R. Shayakhmetov, E. Korznikova, G. Khalikova, R. Mulyukov, Influence of Constrained High-Pressure Torsion on Microstructure and Mechanical Properties of an Aluminum-Based Metal Matrix Composite, JOM (2020) 10.1007/s11837-020-04152-1

[44] M. Kawasaki, J.-K. Han, D-.H. Lee, J.-I. Jang, T. G. Langdon, Fabrication of nanocomposites through diffusion bonding under high-pressure torsion, J. Mater. Res., 33 (2018) 2700-2710.

[45] M. Kawasaki, B. Ahn, H.-J. Lee, A.P. Zhilyaev, T.G. Langdon, Using high-pressure torsion to process an aluminum-magnesium nanocomposite through diffusion bonding, J. Mater. Res., 31 (2016) 88-99

[46] B. Ahn, H.-J. Lee, I.-C. Choi, M. Kawasaki, J.-I. Jang, T.G. Langdon, Micro-Mechanical Behavior of an Exceptionally Strong Metal Matrix Nanocomposite Processed by High-Pressure Torsion, Adv. Eng. Mater. 18 (2016) 1001-1008

[47] J.-K. Han, H.-J. Lee, J.-I. Jang, M. Kawasaki, T. G. Langdon, Micro-mechanical and tribological properties of aluminum-magnesium nanocomposites processed by high-pressure torsion, Mater. Sci. Eng. A 2017, 684, 318.

[48] M. Kawasaki, T.G. Langdon, Using severe plastic deformation to fabricate strong metal matrix composites, Mater. Res., 20 (2017) 46-52

[49] M. Kawasaki, T.G. Langdon, Fabrication of high strength hybrid materials through the application of high-pressure torsion, Acta Phys. Polon. A, 134 (2018) 615-622.

[50] M. Kawasaki, S.-H. Jung, J.-M. Park, J. Lee, J.-I. Jang, J.-K. Han, Mechanical bonding of aluminum hybrid alloy systems through high-pressure torsion, Adv. Eng. Mater., 22 (2020) 1900483

[51] V.N. Danilenko, S.N. Sergeev, J.A. Baimova, G.F. Korznikova, K.S. Nazarov, R. Kh. Khisamov, A.M. Glezer, R.R. Mulyukov, An approach for fabrication of Al-Cu composite by high pressure torsion, Mater. Lett., 236 (2019) 51-55

[52] A. Korneva, B. Straumal, R. Chulist, A. Kilmametov, P. Bała, G. Cios, N. Schell, P. Zięba, Grain refinement of intermetallic compounds in the Cu–Sn system under high pressure torsion, Mater. Lett. 179 (2016) 12-15.

[53] N. Ibrahim, M. Peterlechner, F. Emeis, M. Wegner, S.V. Divinski, G. Wilde, Mechanical alloying via high-pressure torsion of the immiscible Cu50Ta50 system, Mater. Sci. Eng. A, 685 (2017) 19-30

[54] Y. Qi, A. Kosinova, A.R. Kilmametov, B.B. Straumal, E. Rabkin, Plastic flow and microstructural instabilities during high-pressure torsion of Cu/ZnO composites, Mater. Charact. 145 (2018) 389-401

[55] S.O. Rogachev, R.V. Sundeev, V.M. Khatkevich, Evolution of the structure and strength of steel/vanadium alloy/steel hybrid material during severe plastic deformation, Mater. Lett., 173 (2016) 123-126

[56] S.O. Rogachev, S.A. Nikulin, A.B. Rozhnov, V.M. Khatkevich, T.A. Nechaykina, M.V. Gorshenkov, R.V. Sundeev, Multilayer "Steel/Vanadium Alloy/Steel" Hybrid Material Obtained by High-Pressure Torsion at Different Temperatures, Metall. Mater. Trans. A, 48 (2017) 6091-6101

[57] S.O. Rogachev, R.V. Sundeev, N.Yu. Tabachkova, High pressure torsion-induced amorphous phase in a multilayer V-10Ti-5Cr/Zr-2.5Nb/V-10Ti-5Cr hybrid material Mater. Lett. 234 (2019) 220-223

[58] D. Hernández-Escobar, Z.U. Raman, H. Yilmazer, M. Kawasaki, C.J. Boehlert, Microstructural evolution and intermetallic formation in Zn-Mg hybrids processed by high-pressure torsion, Philos. Mag. 99 (2019) 557-584

[59] R.B. Figueiredo, P.H.R. Pereira, M.T.P. Aguilar, P.R. Cetlin, T.G. Langdon, Using finite element modeling to examine the temperature distribution in quasi-constrained high-pressure torsion, Acta. Mater. 60 (2012) 3190-3198.

[60] A. Loucif, R. B. Figueiredo, T. Baudin, F. Brisset, R. Chemam, T. G. Langdon, Effect of ageing on microstructural development in an Al-Mg-Si alloy processed by high-pressure torsion, J. Mater. Sci. 47 (2012) 7815-7820

[61] R.M. Molak, K. Paradowski, T. Brynk, L. Ciupinski, Z. Pakiela, K.J. Kurzydlowski, Measurement of mechanical properties in a 316L stainless steel welded joint, Int. J. Press. Vessel Piping, 86 (2009) 43-47

[62] Y. Huang, M. Kawasaki, T.G. Langdon, Influence of Anvil Alignment on Shearing Patterns in High-Pressure Torsion, Adv. Eng. Mater. 15 (2013) 747-755

[63] Y. Huang, M. Kawasaki, T.G. Langdon, An investigation of flow patterns and hardness distributions using different anvil alignments in high-pressure torsion, J. Mater. Sci. 48 (2013) 4533-4542

[64] Y. Huang, M. Kawasaki, T.G. Langdon, An evaluation of the shearing patterns introduced by different anvil alignments in high-pressure torsion, J. Mater. Sci. 49 (2014) 3146-3157

[65] M. Murayama, Z. Horita, K. Hono, Microstructure of two-phase Al–1.7 at% Cu alloy deformed by equal-channel angular pressing, Acta Mater. 49 (2001) 21-29

[66] X. Xu, Q. Zhang, N. Hu, Y. Huang, T.G. Langdon, Using an Al–Cu binary alloy to compare processing by multi-axial compression and high-pressure torsion, Mater. Sci. Eng. A, 588 (2013) 280–287

[67] Y.W. Ma, K.B. Yoon, Assessment of tensile strength using small punch test for transversely isotropic aluminum 2024 alloy produced by equal channel angular pressing, Mater. Sci. Eng. A, 527 (2010) 3630–3638

[68] I.F. Mohamed, Y. Yonenaga, S. Lee, K. Edalati, Z. Horita, Age hardening and thermal stability of Al–Cu alloy processed by high-pressure torsion, Mater. Sci. Eng. A, 627 (2015) 111–118

[69] Y.W. Ma, J. W. Choi, K. B. Yoon, Change of anisotropic tensile strength due to amount of severe plastic deformation in aluminum 2024 alloy, Mater. Sci Eng. A, 529 (2011) 1– 8

[70] M. Kawasaki, J. Foissey, T.G. Langdon, Development of hardness homogeneity and superplastic behaviour in an aluminum–copper eutectic alloy processed by high-pressure torsion, Mater. Sci Eng. A, 561 (2013) 118–125

[71] X.H. An, Q.Y. Lin, S.D. Wu, Z.F. Zhang, R.B. Figueiredo, N. Gao, T.G. Langdon, The influence of stacking fault energy on the mechanical properties of nanostructured Cu and Cu–Al alloys processed by high-pressure torsion, Scripta Mater.,64 (2011) 954–957

[72] A.K. Parimi, P.S. Robi, S.K. Dwivedy, Severe plastic deformation of copper and Al–Cu alloy using multiple channel-die compression, Mater. Des. 32 (2011) 1948–1956

[73] T. Fujita, Z. Horita, T.G. Langdon, Using grain boundary engineering to evaluate the diffusion characteristics in ultrafine-grained Al–Mg and Al–Zn alloys, Mater. Sci. Eng. A, 371 (2004) 241-250

[74] A. Alhamidi, K. Edalati, Z. Horita, S. Hirosawa, K. Matsuda, D. Terada, Softening by severe plastic deformation and hardening by annealing of aluminum–zinc alloy: Significance of elemental and spinodal decompositions, Mater. Sci. Eng. A, 610 (2014) 17-27

[75] S.V. Divinski, J. Ribbe, D. Baither, G. Schmitz, G. Reglitz, H. Rosner, K. Sato, Y. Estrin, G. Wilde, Nano- and micro-scale free volume in ultrafine grained Cu–1 wt.%Pb alloy deformed by equal channel angular pressing, Acta Mater., 57 (2009) 5706-5717

[76] G.F. Korznikova, K.S. Nazarov, R.Kh. Khisamov, S.N. Sergeev, R. R. Mulyukov, Intermetallic growth kinetics and microstructure evolution in Al-Cu-Al metal-matrix composite processed by high pressure torsion, Mater. Lett.,253 (2019) 412-415

[77] C.C. Hsieh, M.S. Shi, W. Wu, Growth of intermetallic phases in Al/Cu composites at various annealing temperatures during the ARB process, Met. Mater. Int., 18 (2012) 1-6

[78] G. Huang, W. Hou, J. Li, Y. Shen, Development of surface composite based on Al-Cu system by friction stir processing: Evaluation of microstructure, formation mechanism and wear behaviour, Surf. Coat. Technol., 344 (2018) 30-42

[79] L. Yang, B.X. Mi, L. Lin, H.J. Huang, X.P. Lin, X.G. Yuan, Formation sequence of interface intermetallic phases of cold rolling Cu/Al clad metal sheet in annealing process, Mater. Sci. Forum (2013) 600-605

[80] E.O. Hall, The deformation and ageing of mild steel: III Discussion of results, Proc. Phys. Soc. B, 64 (1951) 747-753

[81] N.J. Petch, The cleavage strength of polycrystals, J. Iron Steel Inst., 174 (1953) 25-28

[82] T. Shanmugasundaram, M. Heilmaier, B. S. Murty, V. Subramanya Sarma, On the Hall–Petch relationship in a nanostructured Al–Cu alloy, Mater. Sci. Eng. A, 527 (2010) 7821-7825

[83] D. Tabor, The hardness of solids, Rev. Physics Technology 1 (1970) 145-179

[84] ASM Metals Reference Book, ASM International, Materials Park, OH, 1984

[85] E. Orowan, Fracture and strength of solids, Rep. Prog. Phys., 12(1949) 185- 232

[86] S. Alexandrov, E. Lyamina, Extension of Orowan's method to analysis of rolling of three-layer sheets, Procedia Eng., 207 (2017) 1391-1396

Captions

Fig. 1 The vertical cross-section of the Al-Cu system after HPT processing at room temperature under a pressure of 6.0 GPa for 20, 50, 150 and 200 turns

Fig. 2 SEM BSE images of the Al-Cu-Al sample after 20 turns. a) an overall image of the central region, with enlarged images of the microstructure in b) Al and c) Cu regions. Microstructure image in the edge region d) and e).

Fig. 3 SEM BSE cross-sectional images of the Al-Cu-Al sample after 200 turns. (a) an overall image of central region, showing misalignment between the upper and lower anvils (arrows mark the centres of each anvil) with enlarged images of the microstructure (b). An overall microstructure image in the edge region (c) and high magnification images showing the formation of nano-lamellar structure (d) and intermetallic phases (e).

Fig. 4 STEM bright-field images of the microstructure taken at the disk edge after HPT for 20 turns (a) low magnification and (b) high magnification. (c) HAADF image of the microstructure with marked place of the line EDX scan with corresponding scanning results (d) as a plot of atomic percentage with respect to the scanning distance for Cu and Al elements.

Fig. 5 STEM images taken at the disk edge after HPT for 200 turns showing (a) an overall image of lamellar structure, (b) HAADF image showing the distribution of Al and Cu elements in this lamellar structure, (c) high magnification image of a bimodal structure and (d) HAADF image and a corresponding composition maps of Al and Cu.

Fig.6 (a) SAED patterns taken at the disk edge after HPT for 200 turns and (b) a dark field image from Al_2Cu (110) ring.

Fig. 7 XRD patterns from Al-Cu-Al system in an initial state and after HPT for 20, 50, 150 and 200 turns.

Fig. 8 Microhardness distributions maps for the Al-Cu-Al system after HPT for 20, 50, 150 and 200 turns.

Fig. 9 Typical tensile engineering stress-strain curves for Al-1050 and 99.95Cu alloys in initial states and after HPT processing together with curves for the Al-Cu-Al system after HPT for 20, 50, 150 and 200 turns.

Table 1 The results of engineering tensile tests for initial materials and the Al-Cu-Al nanocomposites fabricated by HPT

Sample	YS [MPa]	UTS [MPa]	Elongation [%]
Cu as-annealed	220 ± 5	280 ± 11	14 ± 4.8
Al as-annealed	70 ± 3	90 ± 5	11.5 ± 6.1
Cu HPT 10 turns	430 ± 11	525 ± 15	4 ± 2.0
Al HPT 10 turns	110 ± 7	200 ± 14	10.3 ± 3.1
Al-Cu-Al HPT 20 turns	280 ± 21	420 ± 30	3.1 ± 1.1
Al-Cu-Al HPT 50 turns	370 ± 27	460 ± 25	1.5 ± 0.6
Al-Cu-Al HPT 150 turns	540 ± 23	710 ± 34	1.7 ± 0.3
Al-Cu-Al HPT 200 turns	680 ± 22	910 ± 16	2.2 ± 0.5

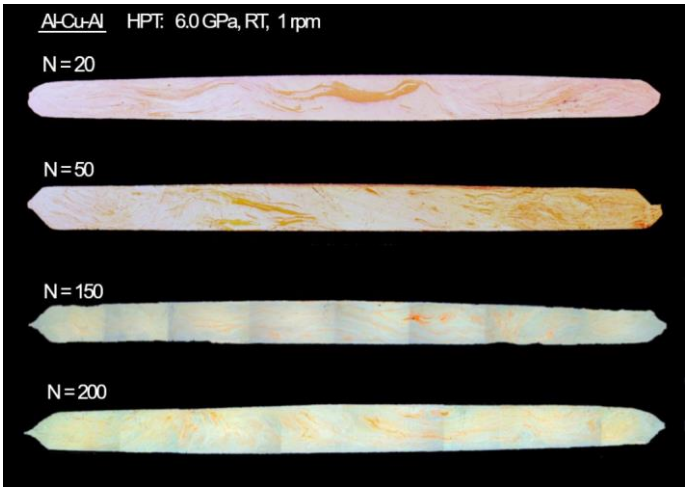

Fig. 1 The vertical cross-section of the Al-Cu system after HPT processing at room temperature under pressure of 6.0 GPa for 20, 50, 150 and 200 turns.

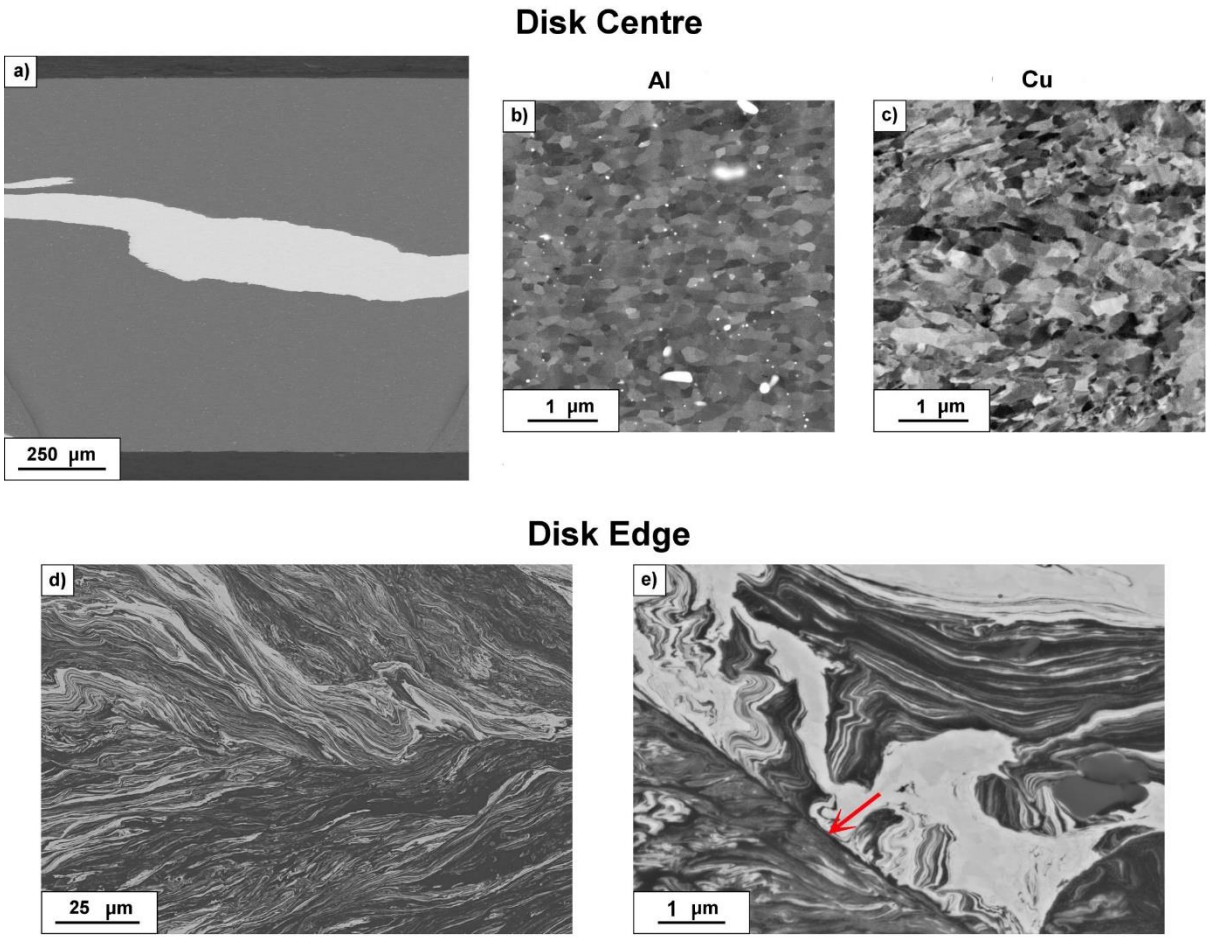

Fig. 2 SEM BSE images of Al-Cu-Al sample after 20 turns. (a) an overall image of central region, with enlarged images of the microstructure in (b) Al and (c) Cu regions. Microstructure images in the edge region (d) and (e).

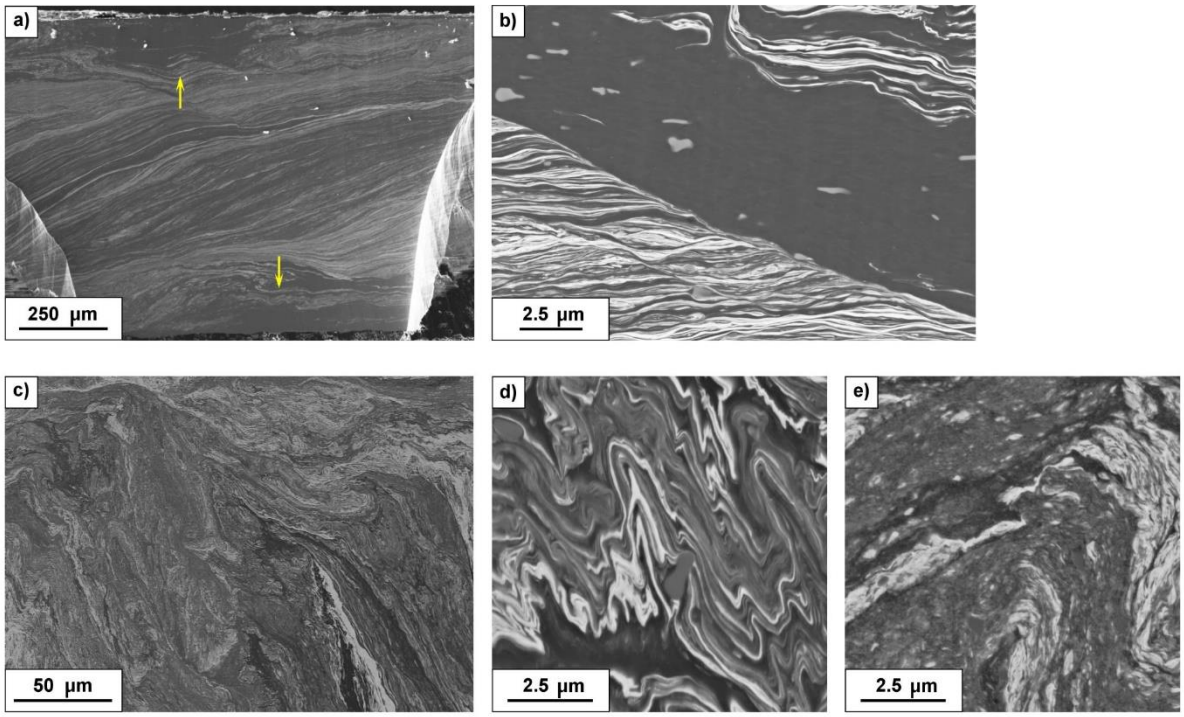

Fig. 3 SEM BSE cross-section images of Al-Cu-Al sample after 200 turns. (a) an overall image of central region, showing misalignment between the upper and lower anvils (marked centres of each anvil) with enlarged images of the microstructure (b). An overall microstructure image in the edge region (c) and high magnification images showing the formation of nano-lamellar structure (d) and intermetallic phases (e).

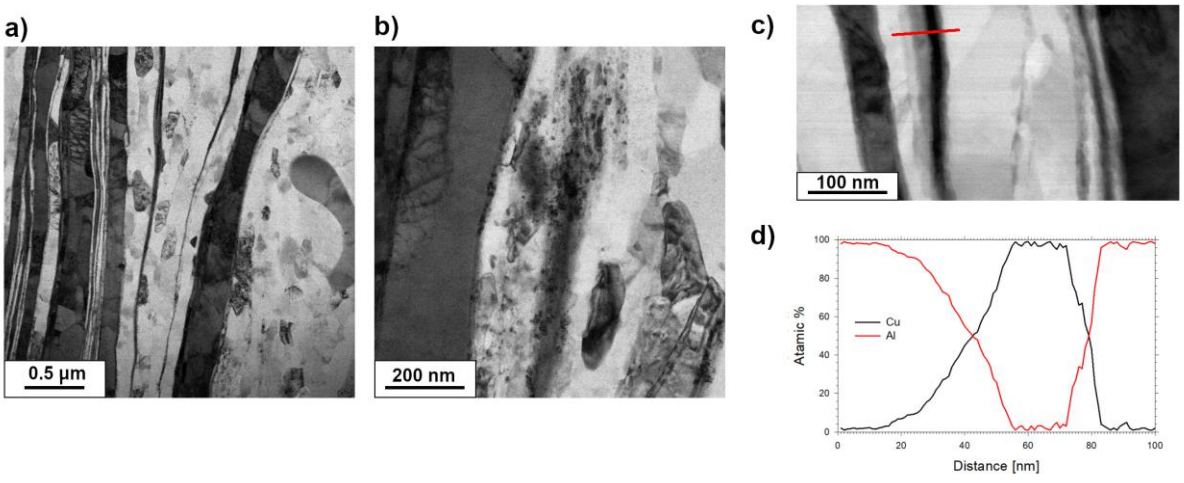

Fig. 4 STEM bright-field images of the microstructure taken at the disk edge after HPT for 20 turns (a) low magnification and (b) high magnification. (c) HAADF image of the microstructure with marked place of the line EDX scan with a corresponding scanning results (d) as a plot of atomic percentage with respect to the scanning distance for Cu and Al elements.

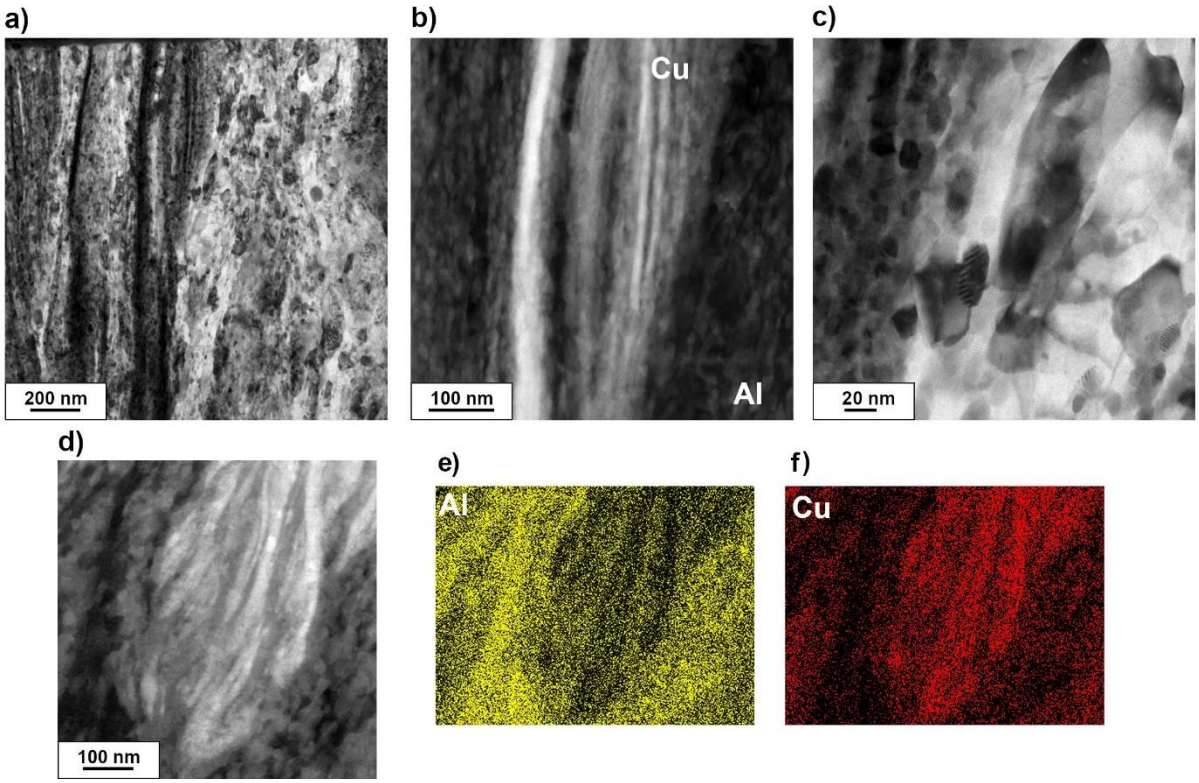

Fig. 5 STEM images taken at the disk edge after HPT for 200 turns showing (a) an overall image of lamellar structure, (b) HAADF image showing the distribution of Al and Cu elements in this lamellar structure, (c) high magnification image of a bimodal structure and (d) HAADF image and a corresponding composition maps of Al and Cu.

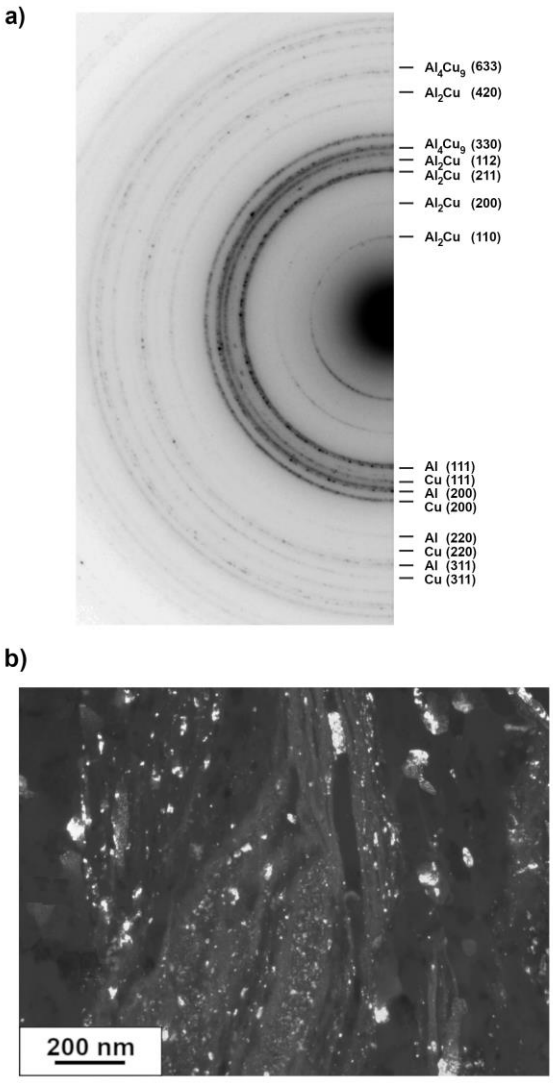

Fig.6 (a) SAED patterns taken at the disk edge after HPT for 200 turns and (b) a dark field image from Al_2Cu (110) ring.

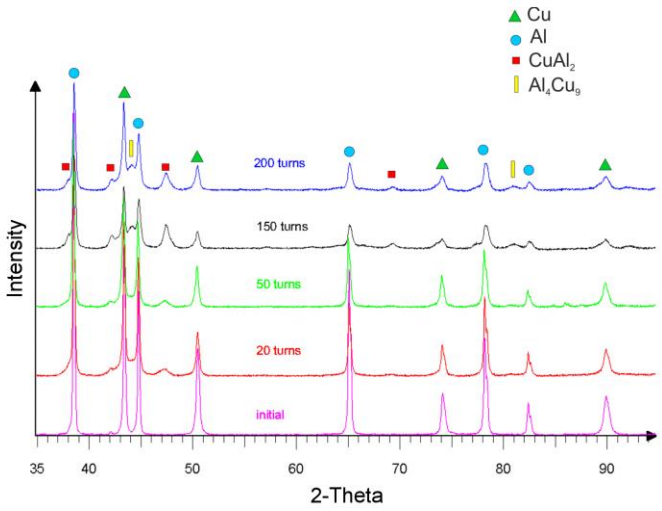

Fig. 7 XRD patterns from Al-Cu-Al system in a initial state and after HPT for 20, 50, 150 and 200 turns.

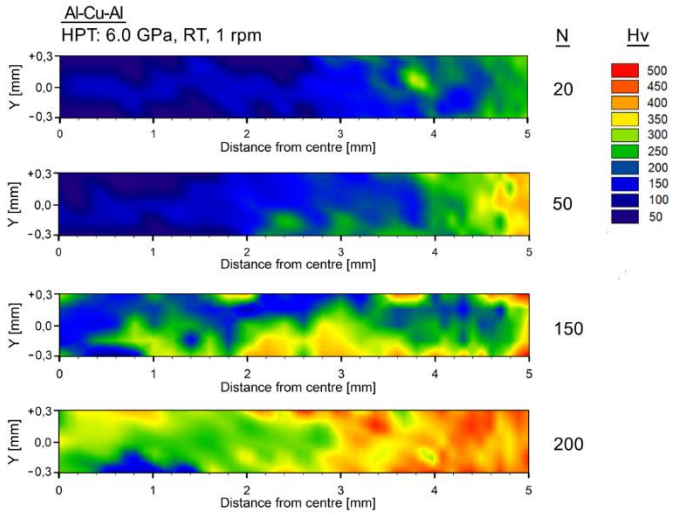

Fig. 8 Microhardness distributions maps for Al-Cu-Al system after HPT for 20, 50, 150 and 200 turns.

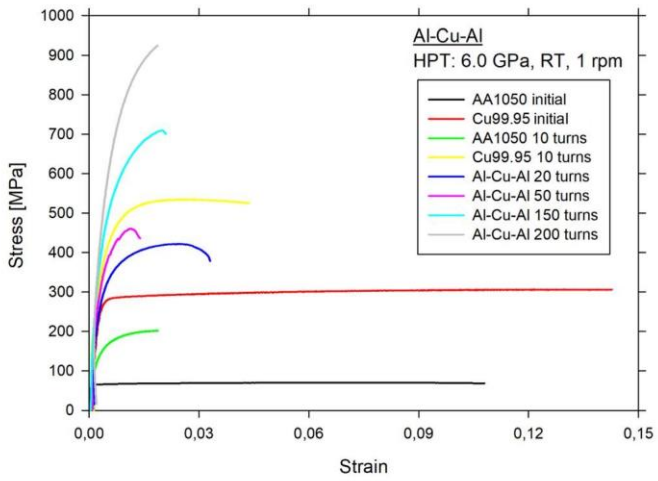

Fig. 9 Tensile test curves for Al1050 and Cu99.95 alloys in initial states and after HPT processing together with curves for Al-Cu-Al system after HPR for 20, 50, 150 and 200 turns.